Evaluation of erosional processes and determining if atolls have aided the formation of polymetallic nodules Caroline Islands, Federated States of Micronesia's Exclusive Economic Zone

Suni McMillen

gmcmil@uw.edu

University of Washington, School of Oceanography

University of Washington
School of Oceanography,
Seattle, WA 98195

Abstract

This project aimed to identify the role nearshore sources of metallics play in the formation of polymetallic nodules in the abyssal planes of the Western Equatorial Pacific. Polymetallic nodules also known as ferromanganese nodules are valuable seafloor features that contain high levels of rare earth metals, of which most notable are manganese and cobalt. The incentive to mine these nodules for their metallics has increased due to the advancement of technology, and demand. The site location for this study was within the exclusive economic zone of the Federated States of Micronesia, and specifically Nam2 Atoll. Three sediment grab samples were collected and an analysis of the historical undercurrents in the region were conducted. X-ray fluorescence spectroscopy was performed on the sediment samples. Two locations contained detectable levels of manganese and one contained cobalt. A particle settling analysis conducted on the sediment grains using Stokes law, calculated the distance of possible travel using the historical undercurrent to model the trajectory of the grains. A conservative time needed to reach the atoll, utilizing only the undercurrents, is 71.2 days. The largest grains were calculated to settle in 19 days while the smallest could stay suspended for several millennia. This study site has had evidence of turbidity currents since the Miocene, and by comparing studies it was determined that a turbidity current from Nam2 could reach approximately 400 km to sites on the abyssal plain. Thus, via a turbidity current, all grain sizes collected could reach the abyssal plains. This study suggests that Co-rich/Mn-rich sediment found at Nam2 Atoll within a wide range of grain sizes, could aid in the formation of polymetallic nodule, (PMN). This would be made possible through transport via undercurrents for smaller sizes and the effects of a large sediment gravity flow for larger grain sizes. These findings potentially increase the locations where mineable amounts of polymetallic nodules could be found globally.

Plain English Summary

Polymetallic nodules are little rocks on the seafloor that take an extremely long time to form. These rocks are of interest because they contain significant amounts of uncommon and desirable elements that are normally very hard to extract from the earth. This project aimed to find out if metallics found on atolls play a role in their formation. To do this, sediment samples were collected from the study site which was an underwater structure called an atoll. An atoll is essentially an island that is now underwater. Next, an instrument that uses X-rays was used to detect the elemental composition of the sediment collected from three places on the study site to see if it was consistent with what these nodules are typically made up of, specifically cobalt and manganese. This test found that some of the sediment collected did reflect the correct elemental composition with trace levels of cobalt and manganese. Second, a calculation based on the particles characteristics was performed to understand if the grains were small enough to be transported to the location where these nodules form, known as the abyssal plains. This was based on the amount of time it takes for these particles to settle and the deep ocean currents within the area. It was found that only the smaller grain sizes could make it to the abyssal plains using only the deep currents. However, underwater avalanches also known as turbidity currents have been common in this area for the past 23 million years and their remnants in this area have been studied. Knowing this, an analysis of these kinds of avalanches was performed. It was determined that an atoll of the size in our study, could produce a turbidity current of 400 km conservatively. This means that the larger grain sizes that would normally not make it to the abyssal plains could now make it by travelling in a turbidity current. Putting it together, sediment containing vital elements for nodule formation can make it to their formation site through deep currents if the grain size is small and through underwater avalanches if large potentially helping form more of the nodules. All in all, this study suggests that when extrapolated to the global ocean, these nodules could be found in many more places than originally thought.

Introduction

Background

Polymetallic nodules (PMN) also known as ferromanganese nodules are an amalgamation of different rare earth elements (REE). They present as stones between <1 to >10 cm in diameter on the seabed (Belkin, et al. 2021; Hein et al., 2020). PMN were first discovered by the *Challenger* expedition in 1872 and were rediscovered in 1878 during the *Vega* expedition (Belkin et al., 2021). PMNs are primarily made from manganese, cobalt, iron, and often contain notable levels of nickel, copper, and titanium (Kuhn et al., 2017). Additionally, the variability in their composition can differ slightly between ocean basins depending on the dominant source of the metallics (Valsangkar & Rebello, 2016). Currently, their presence has been well documented in the Clarion-Clipperton zone, the Cook Islands, and the Central Indian Ocean Basin (CIB) (Kuhn, et al. 2017).

Over the past century, interest in the nodules has wavered due to their inaccessibility, often located at depths of 3000 m or more. However, deep sea mining has gained momentum in the last 30 years as technology has greatly improved (Bath, 1989; Wakefield Myers, 2018). In 2024, a major turn of events occurred in the science world when researchers discovered that PMNs could possibly be creating dark oxygen through seawater electrolysis (Sweetman et al., 2024). While this discovery is exceedingly new and has been put under great scrutiny, it made waves within the greater science community and has renewed interest in PMN formation (Nakamura, 2024).

PMNs primarily form through the precipitation of sediment and metallics from hydrothermal and terrestrial sources (Hein et al. 2020; Kuhn et al., 2017). The formation process of PMNs begins with a core, e.g., a small hard piece of detritus <1 to >8 cm in diameter, that the metallic particles then precipitate on to (Usui et al., 1993). The nucleus allows for layered growth

structures (LGS) of the metallics to form; singular LGS are around nm to μm in thickness (Wegorzewski et al., 2020). Redox reactions between the LGS allow for the layers to become dense through the generation of columnar growth structures. These structures are defined by the nodule's Mn to Fe ratio, low Ni content, usually high Co concentrations, and prominent levels of other REE (Wegorzewski et al., 2020). This process of layering sediments is accepted as a diagenetic source of PMNs from which they grow over millions of years. Additionally, each of the LGS in a nodule reflects the environmental conditions in which the nodule formed in (Hein et al., 2020; Wegorzewski et al., 2020).

A case study on PMN formation in the South China Sea (SCS) found the rates of sedimentation were much higher than in the open ocean, partially due to the amount of sediment sources (Guan et al., 2017). This made the SCS a potentially unfavorable place for PMN formation (Guan et al., 2017). However, this study also suggested that PMNs in the SCS could exhibit higher growth rates and avoid getting buried (Guan et al., 2017). This research provides evidence for the theory that erosion could aid in nodule formation (Guan et al., 2017). Erosion from underwater structures, such as guyots and atolls, is common globally due to their abundance. The EEZ of the Federated States of Micronesia, specifically the Caroline islands, are a uniquely qualified research site because of many atolls and guyots supplying sediment. However, unlike in the SCS there is not a fluvial source of sediment that could bury juvenile nodules (Guan et al., 2017). Many of the atolls and guyots in the Caroline islands do not have names, so for the purposes of this study, our team has given the atoll of importance to this project the name Nam2 Atoll (Fig. 1). Nam2 Atoll is likely an excellent diagenetic source for PMNs due to the potential for cobalt and ferromanganese crusts, prominent bottom currents, steep slopes, and its relatively proximal distance to the abyssal plains.

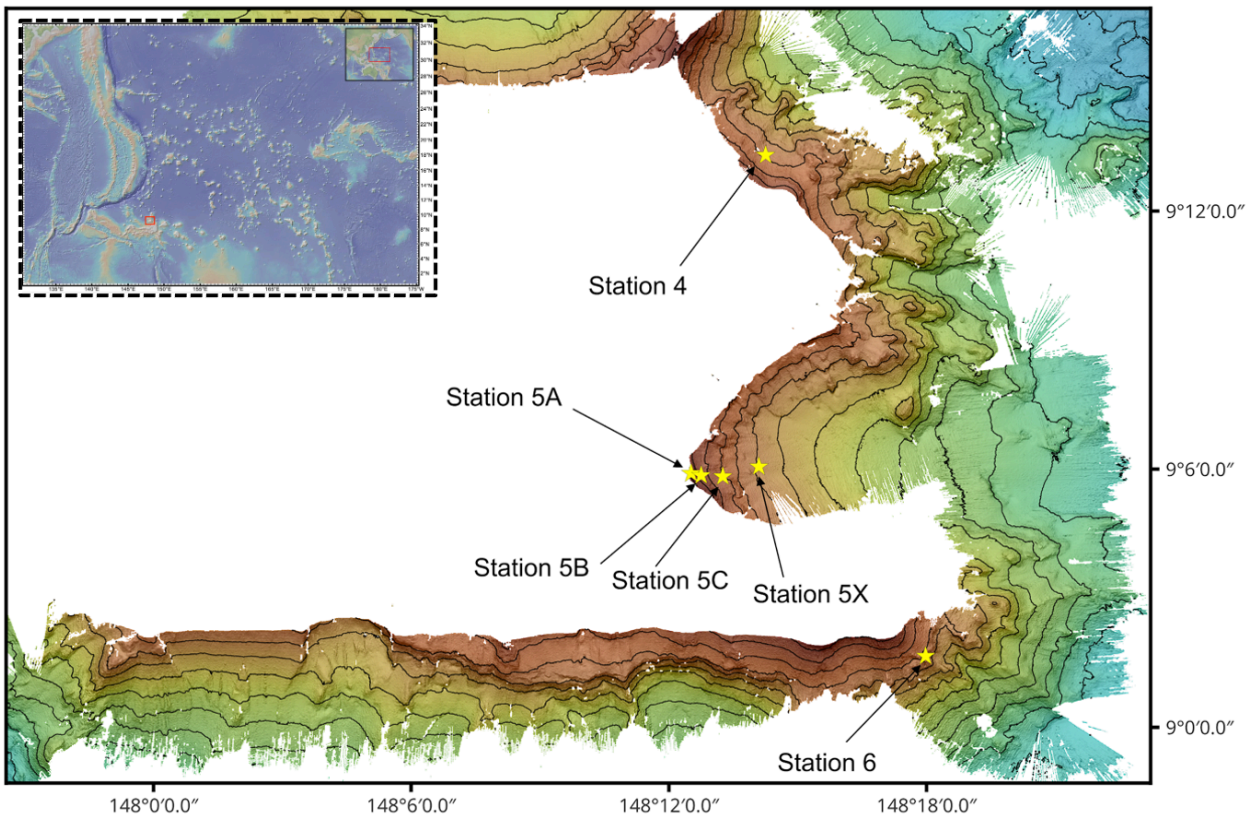

Figure 1. Map of bathymetry around Nam2 Atoll. Yellow stars represent sediment grab site locations on the atoll. Top left sub-plot indicates this atoll's location on larger scale map with small red box. This study used samples from Station 4, Station 5a, and Station 6. Image created using multibeam sonar and processed using QPS-Qimera and QGIS and in GeoMappApp (GEB CO Data & Figure contributed and modified from S. Agopsowicz).

I suspect that structural failures in the slopes of Nam2 Atoll have previously suspended cobalt and manganese-rich sediment into the water column through erosional processes. Once suspended, the sediment was vulnerable to the North Equatorial Undercurrent (NEUC) which relocated them to the abyssal plains which are located 200 – 600 km west of Nam2 Atoll. At the plains the particles could then aid in nodule formation by providing a site of nucleation and minerals to feed the diagenetic process. I hypothesized that sediment samples collected from the flanks of Nam2 Atoll would contain detectable amounts of Co and Mn along with other REEs. Additionally, a model of historical undercurrent velocities would show adequate strength to transport finer grain sizes >200 km to the abyssal plains. In the event that the current velocities

were not strong enough, I made a secondary hypothesis that sediment gravity flows could aid the transport of sediment to the abyssal plains.

Site Review & Supported Hypothesis

The Nam2 Atoll was chosen as the site for this study as it is located near the NEUC, is derived from Co-rich oceanic lithosphere, and is located near an abyssal plain region of the North Western Equatorial Pacific. Mn and Co are found in the crust of the Pacific Ocean at mineable amounts and contain high levels of Ni and Cu (Novikov et al., 2017). The Magellan seamounts, which are located 1000 km north of Nam2 Atoll, present high levels of Co-rich ferromanganese crust (Melnikov & Pletnev, 2013; Novikov et al., 2017). The Magellan seamounts are in close enough proximity to Nam2 Atoll that it is reasonable to assume that they share this trait of Co-rich ferromanganese crusts.

In order to suspend these metallics from the crust, a large erosional event must occur. In atolls and guyots, tsunamigenic landslides are caused by two different categories of failures, endogenic and exogenic (Keating & McGuire, 2000). Endogenic failures are usually caused by the foundation upon which the volcano sits, becoming unstable. Exogenic failures come from the structural integrity of the atoll or guyot becoming compromised, often due to an intrusive heat source (Keating & McGuire, 2000). Either category of failure could result in a sediment gravity flow which would suspend the sediments and their metallics with it throughout the bottom boundary layer. These sediments would then become vulnerable to transport by the undercurrents in the region (Baldwin et al., 2017; Keating & McGuire, 2000).

Sediment gravity flows and specifically turbidity currents have been present in the Caroline Basin since the early to mid-Miocene and have produced previously mapped sediment waves (Baldwin et al., 2017). Turbidity currents are a vital part of this research as they are the

only type of sediment gravity flow capable of reaching immense distances (Mountjoy et al., 2018). Therefore, they offer a secondary process in which the sediments from Nam2 and surrounding atolls could travel the distance to the abyssal plains, which is ~400 km. The size of a turbidity current is dependent on the amount of sediment that is displaced which in turn is dependent on the instigator of the event, and the size of the structure that is failing (Schulz et al., 2012). Since atolls and guyots are fully submerged structures, the main process that would create such events would be earthquakes or structural failures within the atoll (Keating & McGuire, 2000). An example of a turbidity current whose size is appropriate is a turbidity current from Taiwan. This event was a result of hyperpycnal river discharge and it transported sediment over 460 km (Garvey et al., 2017). A turbidity current produced by seismic activity in New Zealand transported sediment over 680 km (Mountjoy et al., 2018).

The most prominent undercurrent near the Nam2 Atoll is the eastward flowing NEUC, which is most significant near 9˚N, 13˚N, and 18˚N across the Pacific Ocean (Qiu et al., 2013) (Fig. 2). Nam2 Atoll is located at 9˚N, at the center of this particular jet (Fig. 2; Fig. 3). Additionally, the undercurrent velocities at the relative location are ~3 cms^{-1}(Qiu et al., 2013). This further suggests that these undercurrent jets play a vital role in sediment transportation and deposition across the Equatorial Pacific (Qiu et al., 2013).

Table 1. Record of the sample site (station), depth of sample, and number of sub samples for each site. (Corresponds to sites shown in Fig. 1).

Station	Coordinates	Depth of grab (m)	Sub-samples per grab
4	(148˚ 14’ 15” E, 9˚ 13’ 18.12” N)	1032.7	14
5a	(148˚ 12’ 30.96” E, 9˚ 5’ 54.24” N)	182.6	14
6	(148˚ 17’ 58.56” E, 9˚ 1’ 39.36” N)	1040.7	38
Real PMN	N/A	N/A	6

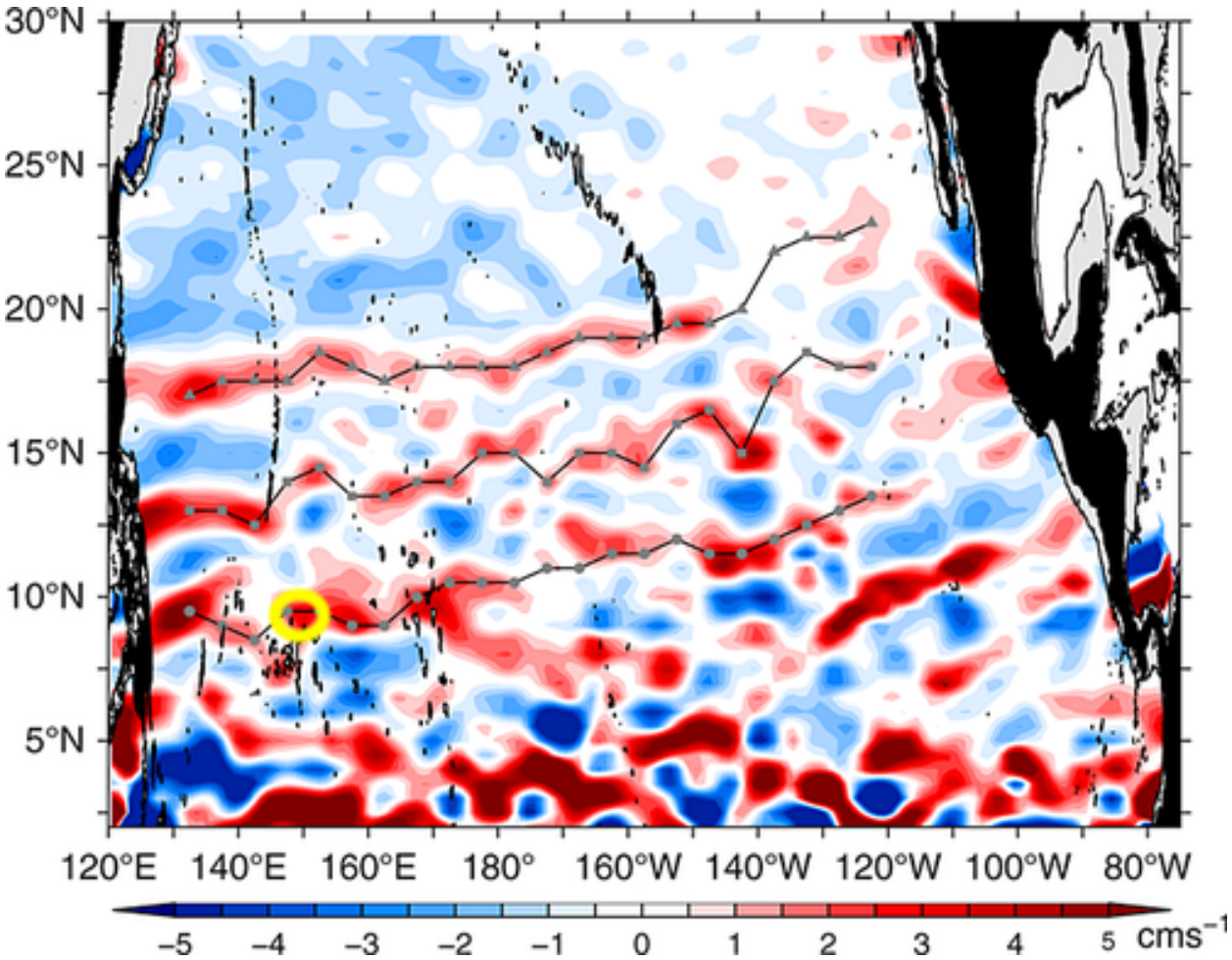

Figure 2. The average velocity of the undercurrents across the equatorial Pacific. The yellow circle is the area of interest, and approximate location of Nam2 Atoll. (Modified from Qiu et al., 2013).

Methods

Sediment Grabs Samples

Grab sample locations were determined before the cruise and chosen with the intention to collect samples at locations where the angle of the slopes was similar. Additionally, the sites were chosen to have a steep angle to stay consistent with what would be suspended during a turbidity current. Sampling at Nam2 Atoll using a Shipek grab sampler was conducted on January 1, 2025, through January 2, 2025. Once at the atoll, the ship was directed to the predetermined sediment grab locations (Stations). Of the six stations where sediment grabs were

collected, Stations 4, 5a, and 6 were used in this study (Figure 1.). Sediment samples were refrigerated at (4 ˚C) until the research cruise had concluded. Due to the resistance of metals to deterioration the samples were transported and stored at room temperature (~23˚C) until they arrived in Seattle, WA. Forty-eight hours after arriving in Seattle the sediment samples were laid out on trays and baked at 176˚C for 20 minutes to dry out the samples.

X-ray Fluorescence

In order to determine the elemental composition of the samples and determine if they contained Mn and Co, X-ray fluorescence (XRF), a form of spectroscopy and works as such, was performed. XRF was chosen because it requires minimal sample preparation and is a relatively quick process. The device sends an X-ray at the sample, exciting the electrons which jump to a higher energy state. When they lose the energy and return to their original position, they produce a photon of a wavelength distinct to each element. The XRF machine used in this study was the Bruker M4 Tornado Micro-XRF which performs energy dispersive XRF (ED-XRF). This means that the photon released is measured directly by an array of detectors allowing for the power of the machine to be lower and take less time. Once the photon is detected and the element is determined based on its wavelength, the machine sends it to a linked computer for processing and categorization. Elements that were not selected to be quantified were still included but are listed as “unquant.” in the tables and data.

For each location that a sediment grab was collected, three sub samples that showed a charactered of the larger sample were collected and XRF was performed on them (Table 1). Since XRF can only pick one point to send the X-ray to at a time, a slide consisting of a diverse and representative portion of the sub sample (i.e., 4a, 4b, 4c, 5a, etc.) was made (Figure 3; Table 3). In this case the sub sample was created by sticking individual grains to a piece of tape then

placing the tape onto a glass slide then placing that into the XRF. Furthermore, once looking at the individual grains through the guide camera on the XRF, specific grains were chosen to X-ray (Figure 4). This meant that for some locations XRF was performed up to 18 times on one slide to ensure that a representative quantity of grains was sampled. Additionally, a real PMN was acquired before deployment from an unknown location, and part of the nodule was ground down and tested using XRF as a control subject. The raw data produced by the XRF was a spectrogram and this information was converted into a pie chart in Excel to be visualized (Figure 5). Finally, since the XRF produced up to 18 spectrograms for one slide, the data had to averaged first across the slide, then across the sub sample, and finally across the station (Table 2).

The composition of PMNs, varies between ocean basins. Due to a difference in the primary source of metallics to the nodule which make up their LGS'. For this reason, Mn and Co were not the only metals tested. The XRF was also used to test for the elements Ca, Au, Ag, Fe, Mg, and Si. Additionally, after further consideration, for the real PMN, Ni and Cu were added to the test. Part of the goal of testing all of these elements was to study the petrology of the rocks chosen for XRF.

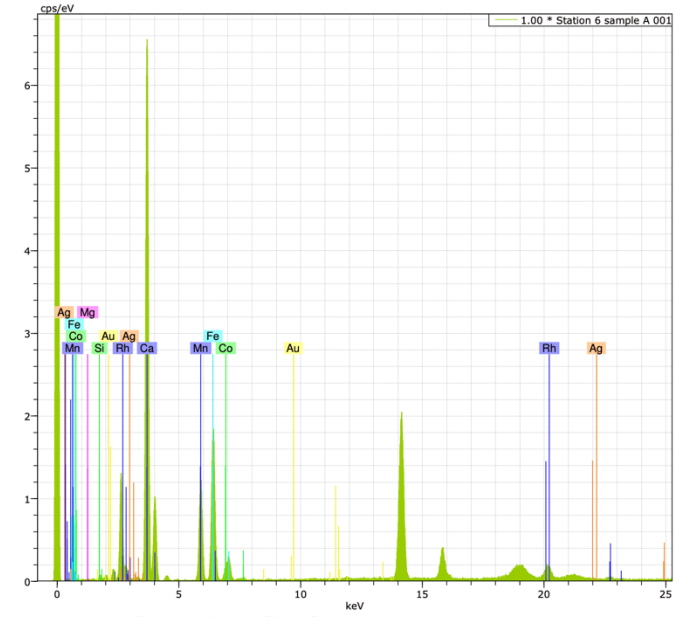

El	AN	Series	unn. C [wt.%]	norm. C [wt.%]	Atom. C [at.%]	Error (1 Sigma) [wt.%]
Mn	25	K-series	3.46	11.69	8.93	0.00
Co	27	K-series	0.25	0.84	0.60	0.00
Rh	45	K-series	0.00	0.00	0.00	0.00
Si	14	K-series	0.36	1.23	1.84	0.00
Ca	20	K-series	20.89	70.60	73.96	0.00
Fe	26	K-series	3.74	12.64	9.51	0.00
Mg	12	K-series	0.88	2.99	5.16	0.00
Au	79	L-series	0.00	0.00	0.00	0.00
Ag	47	K-series	0.00	0.00	0.00	0.00
		Total:	29.58	100.00	100.00	

Figure 3. X-ray fluorescence (XRF) raw spectrum from Station 6 sample A sub-sample 001. The elements present in the sub-sample are listed on the graph and flagged by color. The X-axis can be interpreted as energy, and Y-axis can be interpreted as number of photons. Energy Dispersive XRF (ED-XRF) uses Rhodium as the anode material in the X-ray tubes. This is why it is present in this spectrum and some of the results. However, its percentage has been manually set to 0 in the tables and corresponding results.

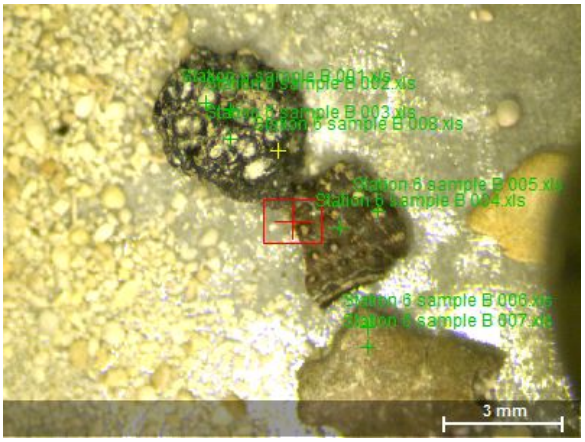

Figure 4. Image of Station 6 sample C sub-sample 001 through sub-sample 7. Green and yellow plus symbols on the sample represent the location where the X-rays were directed, with their accompanying labels, also in green.

Historical Current Velocities

In order to understand the history of undercurrent behavior in the region of Nam2 Atoll, the data was sourced and processed. This study used gridded monthly averaged ocean velocity data from the Physical Oceanography Distributed Active Archive Center (PODAAC) which is funded by NASA through JPL (ECCO Consortium et al., 2021). The dataset dates range from 1992 until 2018, and the full dataset was used. Originally, the current data was categorized by location and linked to a tile which represented a section of Earth's surface. This tile was a part of a native grid system which, when combined, spanned the globe. As a result, to acquire the right tile containing the specific area of Earth which encompassed the study site of this project, python code was written in anaconda to download the specific data. The undercurrent velocities were processed using python code in a Google Collab notebook and graphs were made using the same workspace.

Particle Settling Analysis

The time a sediment particle needed to settle to the seafloor was required. Therefore, the Stokes settling velocity equation was calculated for a representative quantity of the particles (Stokes, 1856). Stokes settling equation relies on the radius of the particle in question and the particle density. To find the characteristic particle radius per sub sample, a small ruler was used to find the difference in size between the largest and smallest particles on each slide. This was possible due to the fact that the majority of the particles that contained the desired elements were relatively large. Using the Euclidean distance formula, the radius was derived from the measurable dimensions of the sediment (Liberti et al., 2014; Anjos & Lasserre, 2011). It is important to note that this method assumes a spherical particle and is a characteristic of the grain sizes sampled. Due to the nature of the Euclidian distance formula, the sub sample had to be

relatively consistently sized. Otherwise, the difference in size between the largest grain and the smallest would skew the results. To avoid this occurring, Station 6 sub sample B, was split into two calculations due to the large difference in particle dimensions within the initial sub sample (Liberti et al., 2014; Anjos & Lasserre, 2011):

$$D = \sqrt{(x_2 - x_1)^2 + (y_2 - y_1)^2 + (z_2 - z_1)^2} \qquad \text{Eq. 1}$$

The particle density was split up into what was determined as basalt-like and calcium carbonate-based sediments. The density of these two classifications was determined by averaging reported particle densities for basalt clay-sized particles and rocks for $CaCO_3$-based sand-sized particles. The reasoning for using an averaged density of basalt clay-sized particles and rock was that the larger particles in the samples, which also happen to contain the target elements, were structurally weak and turned into powder under pressure. For $CaCO_3$ based sediments, the largest grain sizes were of sand-size and the smallest were clay-sized particles, so the same method was applied. The value used for the particle density for $CaCO_3$-based sediment was 2630 kg/m^3 (Snoeckx & Rea, 1994). The final value used for the particle density of basalt-like material was 2949 kg/m^3 (Reijmer et al., 2025; Aumento et al., 1977). The final particle density for a real PMN was 2000 kg m^{-3} (Turner et al., 2019) (Table 3). Sediment gravity flows are more than likely to break some of these particles and suspend some of them into the water column further justifying this methodology. Once determined, these density values values were plugged into the Stokes settling velocity equation to yield a range of velocities (Moran, 2018):

$$V = \frac{2}{9}\frac{(\rho_p - \rho_f)}{\mu} g R^2 \qquad \text{Eq. 2}$$

(Stokes, 1856)

Where V is the terminal velocity, R is the particles radius, g is the acceleration due to gravity, ρ_p is the particle density, ρ_f is the fluid density, and μ is the fluid dynamic viscosity. For simplicity,

the fluid density was assumed to be 1025 kg m^{-3}, and the fluid viscosity was assumed to be equal to 1 kg m^{-1} s^{-1}. These vertical settling velocities were then compared to the undercurrent velocities from PODAAC to yield the maximum distance that these particles could have traveled. The ocean depth in the plains was assumed to be 4000 m, which is characteristic of the abyssal plains and consistent with GeoMapApp's GEB CO data.

Results

Surface Sediment Grab Samples

Sediment collected at each location had distinct characteristics. Station 4 had larger grains of yellowish calcium carbonate with visibly no darker basalt-like particles (Table 3; Figure 7). The average radius for these particles was 3.17E-03 m (Table 3). The bathymetry at Station 4 was smooth and had a steep angle (Figure 1). Station 5a consisted of almost all yellowish calcium carbonate particles, the average particle radius was 2.26E-03 m, and the bathymetry was flat with a gentler slope (Figure 1; Table 3; Figure 7). Station 6 had a steep slope with complex, rough bathymetry (Figure 1). Station 6 consisted of larger dark and yellow particles with a diverse elemental composition, and the average particle radius was 2.57E-03 m (Figure 7; Table 3).

X-ray Fluorescence

Across the stations, the element that consistently was ranked most abundant in the samples was calcium, in the form of calcium carbonate shells ($CaCO_3$). This was closely followed by elements that were unquantified by the XRF analysis, listed as "unquant." (Figure 3; Figure 5; Table 2). Next in abundance was magnesium, and iron which were detected at all of the stations. Silicon was the last element detected at every location at a level >0.06%. However, more elements were present across the stations at percentages below 0.001% (Table 3; Figure 5).

Cobalt and manganese were present in several of the sediment samples, and prominently at Station 6, which had predominantly basalt-like sediment (Figure 5; Figure 7; Table 4). Other heavy weight elements were found at Station 6 as well, such as iron, and magnesium (Figure 3; Table 3). Station 4 and 5a also contained a wide variety of these atomically heavier metals but in lower percentages (Table 3.). Based on the results of the XRF, samples were determined to be either calcium carbonate based or basaltic based (Table 3; Table 4).

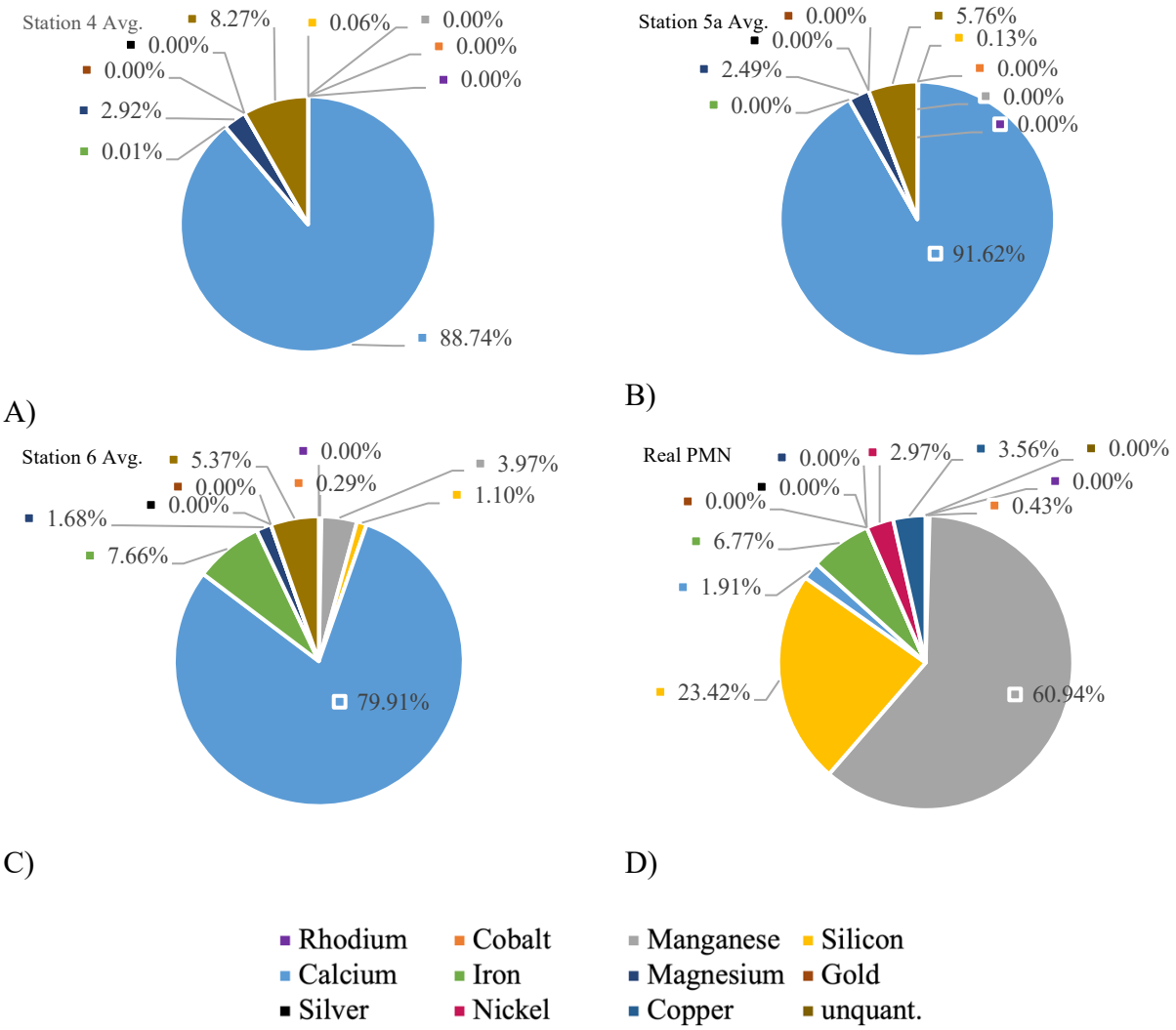

Figure 5. The elemental breakdown of each station averaged over the multiple sub-samples at that location. Some of the elements shown read 0%, which is due to the limitations of the pie chart which cannot illustrate numbers smaller than 0.0001. To see the full elemental breakdown at each station refer to Table 3.

Table 2. Percentage of target elements at each station averaged across each sub sample. Corresponds to Figure 5.

Element	Station 4 Avg.	Station 5a Avg.	Station 6 Avg.	Real PMN Avg.
Rhodium	0	0	0	0
Cobalt	0	0	0.00292	0.00428
Manganese	0.0000245	0	0.0397	0.609
Silicon	0.000343	0.00129	0.011	0.234
Calcium	0.725	0.916	0.799	0.0191
Iron	0.000185	0.0000199	0.0766	0.0677
Magnesium	0.0262	0.0249	0.0168	0
Gold	0	6.57E-06	0	0
Silver	0	0	0	0
Unquant.	0.248	0.0578	0.0540	0.0653

Undercurrent Velocities

The historical undercurrent velocity profile shows prominent undercurrents below 1200 m at specific latitudes over the 26 years of data collection (Figure 6). The undercurrents were weakest just south of the atoll and grow in velocity to the north and south. The undercurrent switches direction at ~8˚N. The undercurrent is strongest with a velocity of 0.12 m s^{-1} at 12˚N where it is directed to the west (towards Asia). The undercurrents are weakest at ~8˚N which is consistent with the latitude where the undercurrents switch directions. The undercurrent velocity at this latitude is 0.065 m s^{-1}. Since the monthly data has been averaged, the undercurrent remains faintly directed westward.

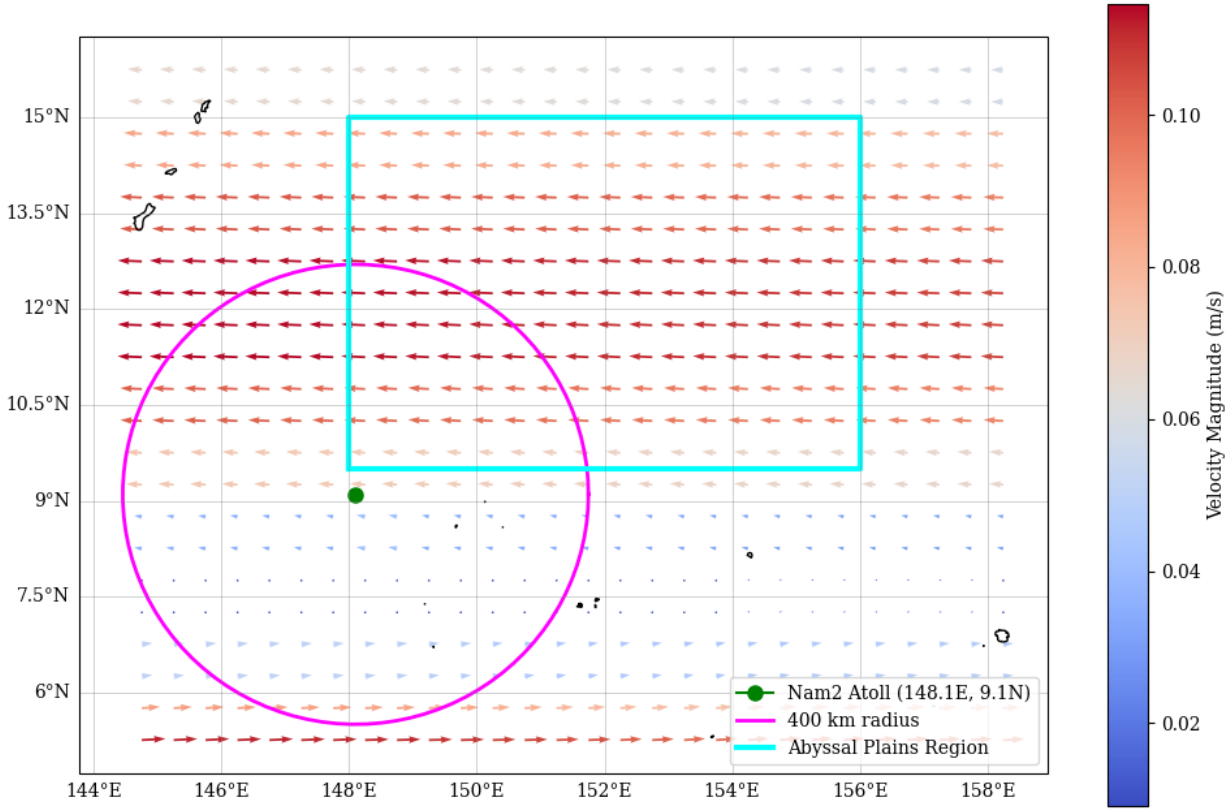

Figure 6. Undercurrent velocity profile of depths below 1200 m averaged monthly from 1992 to 2018. The green dot is the location of Nam2 Atoll. The magenta ring is a 400 km radial distance from the atoll representing the possible distance that extreme turbidity currents and sediment gravity flows reach. The cyan blue box highlights the area near Nam2 that is abyssal plains and suited for PMN formation (Garvey et al., 2017; Mountjoy et al., 2018; ECCO Consortium et al., 2021).

Particle Settling Analysis (Stokes)

The grain size analysis using Stokes law on a wide range of particle radii, yielded settling times of 19 to 264 days assuming an ocean depth of 4000 m. Next, calculation assuming a depth of 4000 m, current speed of 0.065 m s^{-1}, and a distance of 400 km yielded a conservative time to reach the abyssal plains at 71.2 days. This can be interpreted as the amount of time needed for the current to move a sediment grain from the atoll to the abyssal plains without the aid of a sediment gravity flow. Horizontal or lateral movement was not considered as the abyssal plains exist in every direction from the atoll except south. While the larger grainsizes would not reach

the the plains before settling out of the water column only utilizing undercurrents – each of the three stations produced at least one sample whose grain size characteristic was small enough to reach the plains (Table 3). These are samples 4 B, 5a C, and 6 B; Station 5a B produced a settling time of 551 days which given the right conditions could also reach the plains (Table 3). With the aid of a turbidity current, some sediment from every station would reach the plains. In the case of 5a B & C, the sediment is capable of staying suspended in the water column for over one-hundred-thousand years and cross the pacific multiple times.

Table 3. Grain size analysis results & settling times for sediments. Assumes and ocean depth of 4000 m, ocean density of 1025 kg m^{-3}, and fluid viscosity of 1 kg m^{-1} s^{-1}. A, B, and C refer to the sample at the specific sub-sample from the Station (4, 5a, or 6). The minimum time needed to reach the atoll is 355 days at the averaged undercurrent velocity; compare this to the last two columns. The radius column was not found through direct measurement but instead, derived through a calculation of measurable dimensions including the diameter of the particle in question.

Station & Sample	Type of rock	Accepted density (Kg m^{-3})	Radius of samples (m)	Stokes Settling Velocity (m s^{-1})	Time to settle (days)	Distance w/ Only Currents (km)	Distance w/ Turbidity Currents
4_A	$CaCO_3$	2630	4.63E-03	7.51E-02	6.16E+01	5.18E+01	4.52E+02
4_B	$CaCO_3$	2630	1.38E-03	6.65E-03	6.96E+02	5.84E+02	9.84E+02
4_C	$CaCO_3$	2630	3.50E-03	4.29E-02	1.08E+02	9.07E+01	4.91E+02
5a_A	$CaCO_3$	2630	2.66E-03	2.48E-02	1.87E+02	1.57E+02	5.57E+02
5a_B	$CaCO_3$	2630	1.55E-03	8.40E-03	5.51E+02	4.63E+02	8.63E+02
5a_C	$CaCO_3$	2630	2.57E-03	2.31E-02	2.00E+02	1.68E+02	5.68E+02
6_A	Basalt-like	2930	3.50E-03	5.09E-02	9.10E+01	7.64E+01	4.76E+02
6_B_Big	Basalt-like	2930	2.25E-03	2.10E-02	2.20E+02	1.85E+02	5.85E+02

6_B_Small	$CaCO_3$	2630	7.08E-04	1.76E-03	2.64E+03	2.21E+03	2.61E+03
6_C	Basalt-like	2930	3.80E-03	5.99E-02	7.73E+01	6.49E+01	4.65E+02
Real PMN	Nodule	2000	1.65E-03	5.75E-03	8.04E+02	6.76E+02	1.08E+03

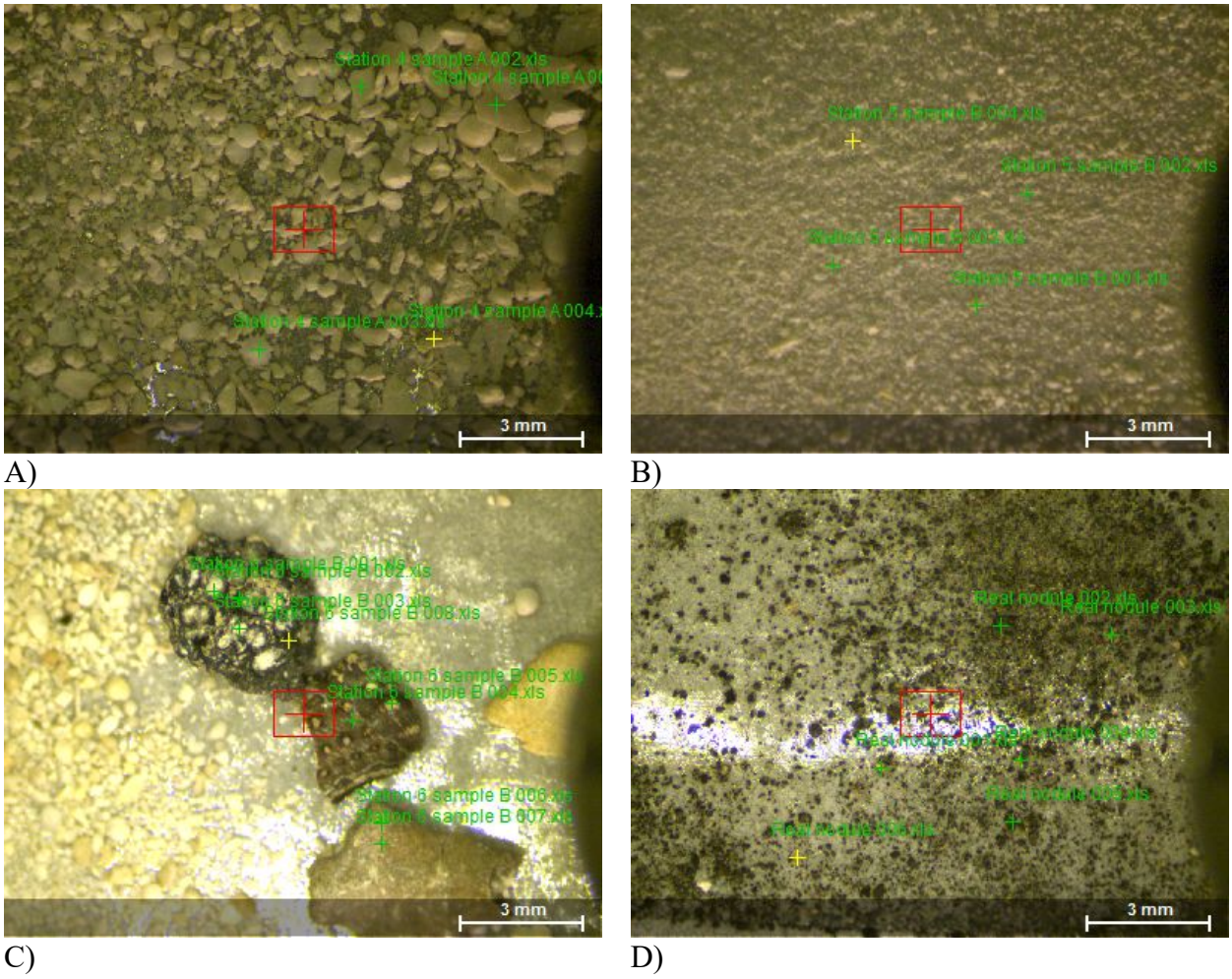

A) B)

C) D)

Figure 7. Example of slides of sub samples from several representative stations. A) Station 4 sub sample A. B) Station 5 sub sample B. C) Station 6 sub sample B. D) Real PMN. The larger dark particles in C were determined to be the basalt-like sediments that contained high levels of metallics (Table 2; Table 3).

Discussion

The results of this study show that manganese was consistently the third or second most prevalent element at each station (Table 3). Cobalt was only detected in Station 6's sediments, and not in a high quantity. This makes it impossible to definitively say that atolls are a consistent reliable source of the element to the abyssal plains. However, it is notable that Station 6 was the steepest station. What is known is, PMNs formed through diagenetic processes tend to show nodules with higher manganese content but lower iron, and cobalt levels (Lenoble, 2000). The process and data described in this study is consistent with diagenetic nodule formation (Table 3). Furthermore, nodules that are formed in the Pacific are known to have much higher concentrations of manganese in comparison to PMNs found in other ocean basins (McKelvey et al., 1983). This study's results, regarding the chemical makeup of the samples, are significant because they show that Nam2 Atoll is a prominent source of manganese to the ocean. However, the same is not true for cobalt. However, this study does not rule out that other atolls and guyots could potentially be a prominent source of cobalt.

Transporting REEs within the sediment to the abyssal plains is essential for PMN formation. The abyssal plains typically have very low sedimentation rates which is key for nodule formation to prevent them from becoming buried as they form. However, these metallics still need to be deposited in the plains for nodule formation to occur. The first method of travel advected by undercurrents found that only smaller grains could reach the plains. Additionally, this study found the NECU jets 4˚ lower in latitude than Qiu et al. (2013), and with double the velocity (Figure 6.). The second method of transport described in this study is a sediment gravity flow in the form of a turbidity current. The distance a turbidity current could travel from Nam2 Atoll was determined by comparing similar sized events form southern Taiwan and New

Zealand. Furthermore, the slopes of Nam2 Atoll show evidence of large failures likely to create sediment gravity flows (Agopsowicz, 2025). A conservative estimate based on these references, indicates that the range of a turbidity current from Nam2 Atoll would be ~400 km. The distance to the abyssal plains was also found to be ~400 km. With the aid of a sediment gravity flow, the characteristic grain size from each station can reach the abyssal plains, making it increasingly possible that past flows aided in nodule formation. Given that Station 4 and Station 6 contained manganese and other REEs, the hypothesis that sediment reaching the abyssal plains aided by turbidity currents have the potential to aid in nodule formation is supported (Table 3 & 4; Figure 4).

PMNs form over 4000-40,000 years so it is increasingly likely, given this time frame, that turbidity currents aid in supplying the metallics necessary for nodule formation. When extrapolated to the whole Pacific Ocean these findings suggest that there are significantly more places where PMN fields could be forming through diagenetic processes. Further research would best be aimed towards studying ocean bottom currents and metallic nanoparticles to gain an understanding of where more PMN fields could be located. Specifically studying metallics from terrestrial sources, atolls, and guyots would be beneficial since this study shows they can contain manganese and other essential REEs. Finally, further research on whether nodules form faster in regions with higher sedimentation would be incredibly useful in mapping regions of potential formation.

Conclusion

This project aimed to understand if metallics originating from atolls could aid in the diagenetic formation of PMNs. The results support our hypothesis, finding that with the aid of a turbidity current, sediment from each sampled location could reach the target distance of 400 km

and beyond. However, bottom currents alone are unlikely to be sufficient unless the grain size is extremely small. Additionally, an elemental analysis showed manganese in the sediment collected form the northern and southern flanks of the atoll (Stations 4 & 6). Cobalt was present in a small quantity at Station 6, located on the southern flank, and is the steepest station. Together these findings strengthen the hypothesis that sediment gravity flows from atolls and guyots potentially aid in PMN formation. The implications of this study are vast as it greatly increases the area of the ocean floor where PMN formation could be observed. Future research would best be aimed at understanding the behavior of inorganic metallics in the ocean, and if PMNs form faster in regions with higher sedimentation rates.

Acknowledgements

I would like to thank the entire undergraduate oceanography mentor team, and especially Dr. Andrea Ogston in her incredible help and support as my advisor. Additionally, the captain, officers, engineers, and crew of the *R/V Thompson* for their support while at sea. Thank you to the University of Washington's School of Oceanography for sponsoring this research. Thank you to the MSE team and specifically Carter Beamish for training me on how to use the X-ray fluorescence machine. Thank you to Dr. Alison Gray for working with me since December of last year on getting historical under current data from PODAAC. Thank you to Dr. Rick Kiel for providing me with a real PMN to have and use for this thesis. Thank you to Dr. Chris Basset for inspiring me to continue learning about the ocean. Finally, thank you to my peer and friend Jood M. AlMokharrak for helping me through this academically tough quarter.

References:

Anjos, M. F., & Lasserre, J. B. (2011). *Handbook on Semidefinite, Conic and Polynomial Optimization*. Springer. http://ebookcentral.proquest.com/lib/washington/detail.action?docID=884131

Aumento, F., Melson, W. G., & et al. (1977). *Initial Reports of the Deep Sea Drilling Project, 37* (Vol. 37). U.S. Government Printing Office. https://doi.org/10.2973/dsdp.proc.37.1977

Baldwin, K. E., Mountain, G. S., & Rosenthal, Y. (2017). Sediment waves in the Caroline Basin suggest evidence for Miocene shifts in bottom water flow in the western equatorial Pacific. *Marine Geology*, *393*, 194–202. https://doi.org/10.1016/j.margeo.2017.07.017

Bath, A. R. (1989, May 1). *Deep Sea Mining Technology: Recent Developments and Future Projects*. Offshore Technology Conference. https://doi.org/10.4043/5998-MS

Belkin, I. M., Andersson, P. S., & Langhof, J. (2021). On the discovery of ferromanganese nodules in the World Ocean. *Deep Sea Research Part I: Oceanographic Research Papers*, *175*, 103589. https://doi.org/10.1016/j.dsr.2021.103589

ECCO Consortium, Fukumori, I., Wang, O., Fenty, I., Forget, G., Heimbach, P., Ponte, & R.M. (2021, April 19). *ECCO Ocean Velocity—Monthly Mean 0.5 Degree (Version 4 Release 4)*. Physical Oceanography Distributed Active Archive Center (PO.DAAC). https://podaac.jpl.nasa.gov/dataset/ECCO_L4_OCEAN_VEL_05DEG_MONTHLY_V4R4

Gavey, R., Carter, L., Liu, J. T., Talling, P. J., Hsu, R., Pope, E., & Evans, G. (2017). Frequent sediment density flows during 2006 to 2015, triggered by competing seismic and weather events: Observations from subsea cable breaks off southern Taiwan. *Marine Geology*, *384*, 147–158. https://doi.org/10.1016/j.margeo.2016.06.001

Guan, Y., Sun, X., Ren, Y., & Jiang, X. (2017). Mineralogy, geochemistry and genesis of the polymetallic crusts and nodules from the South China Sea. *Ore Geology Reviews*, *89*, 206–227. https://doi.org/10.1016/j.oregeorev.2017.06.020

Hein, J. R., Koschinsky, A., & Kuhn, T. (2020). Deep-ocean polymetallic nodules as a resource for critical materials. *Nature Reviews Earth & Environment*, *1*(3), 158–169. https://doi.org/10.1038/s43017-020-0027-0

J.P., L. (2000, January 10). *Polymetallic Nodules*. International Seabed Authority. https://www.isa.org.jm/wp-content/uploads/2022/06/eng7.pdf

Kaikkonen, L., & van Putten, I. (2021). We may not know much about the deep sea, but do we care about mining it? *People and Nature*, *3*(4), 843–860. https://doi.org/10.1002/pan3.10224

Keating, B. H., & McGuire, W. J. (2000). Island Edifice Failures and Associated Tsunami Hazards. *Pure and Applied Geophysics*, *157*(6), 899–955. https://doi.org/10.1007/s000240050011

Kuhn, T., Wegorzewski, A., Rühlemann, C., & Vink, A. (2017). Composition, Formation, and Occurrence of Polymetallic Nodules. In R. Sharma (Ed.), *Deep-Sea Mining: Resource Potential, Technical and Environmental Considerations* (pp. 23–63). Springer International Publishing. https://doi.org/10.1007/978-3-319-52557-0_2

Liberti, L., Lavor, C., Maculan, N., & Mucherino, A. (2014). Euclidean Distance Geometry and Applications. *SIAM Review*, *56*(1), 3–69.

M4 TORNADO. (n.d.). Retrieved February 4, 2025, from https://www.bruker.com/en/products-and-solutions/elemental-analyzers/micro-xrf-spectrometers/m4-tornado.html

McKelvey, V. E., Wright, N. A., & Bowen, R. W. (1983). *Analysis of the World Distribution of Metal-Rich Subsea Manganese Nodules* (Geological Survey Circular 886; Circular, p. 60). United States Department of the Interior. https://pubs.usgs.gov/circ/1983/0886/report.pdf

Melnikov, M. E., & Pletnev, S. P. (2013). Age and formation conditions of the Co-rich manganese crust on guyots of the Magellan seamounts. *Lithology and Mineral Resources*, *48*(1), 1–13. https://doi.org/10.1134/S0024490212050057

Miller, K. A., Thompson, K. F., Johnston, P., & Santillo, D. (2018). An Overview of Seabed Mining Including the Current State of Development, Environmental Impacts, and Knowledge Gaps. *Frontiers in Marine Science*, *4*. https://doi.org/10.3389/fmars.2017.00418

Moran, S. (2018). Chapter 5—Fluid mechanics. In S. Moran (Ed.), *An Applied Guide to Water and Effluent Treatment Plant Design* (pp. 53–58). Butterworth-Heinemann. https://doi.org/10.1016/B978-0-12-811309-7.00005-9

Mountjoy, J. J., Howarth, J. D., Orpin, A. R., Barnes, P. M., Bowden, D. A., Rowden, A. A., Schimel, A. C. G., Holden, C., Horgan, H. J., Nodder, S. D., Patton, J. R., Lamarche, G., Gerstenberger, M., Micallef, A., Pallentin, A., & Kane, T. (2018). Earthquakes drive large-scale submarine canyon development and sediment supply to deep-ocean basins. *Science Advances*, *4*(3), eaar3748. https://doi.org/10.1126/sciadv.aar3748

Nakamura, K. (2024). *Questioning Dark Oxygen Production in the Deep-sea Ferromanganese Nodule Field*. https://eartharxiv.org/repository/view/7819/

Novikov, G. V., Melnikov, M. E., Bogdanova, O. Y., Drozdova, A. N., & Lobus, N. V. (2017). Mineralogy and Geochemistry of Co-bearing manganese crusts from the Govorov and Volcanologist guyots of the Magellan Seamounts (Pacific Ocean). *Oceanology*, *57*(5), 716–722. https://doi.org/10.1134/S0001437017050137

Qiu, B., Rudnick, D. L., Chen, S., & Kashino, Y. (2013). Quasi-stationary North Equatorial Undercurrent jets across the tropical North Pacific Ocean. *Geophysical Research Letters*, *40*(10), 2183–2187. https://doi.org/10.1002/grl.50394

Qiu, Z., Dong, Y., Ma, W., Zhang, W., Yang, K., & Zhao, H. (2020). Geochemical characteristics of platinum-group elements in polymetallic nodules from the Northwest Pacific Ocean. *Acta Oceanologica Sinica*, *39*(8), 34–42. https://doi.org/10.1007/s13131-020-1616-y

Reijmer, J. J. G., De Kruijf, M., Slootman, A., Kranenburg, L. J., & De Boer, R. A. (2025). Experiments on the settling of carbonate sand–mud suspensions. *Journal of Sedimentary Research*, *95*(1), 28–48. https://doi.org/10.2110/jsr.2024.116

Schulz, H., Lobosco, R., & Simoes, A. (2012). *Hydrodynamics: Natural Water Bodies*. BoD – Books on Demand.

Snoeckx, H., & Rea, D. K. (1994). Dry bulk density and CaCO3 relationships in upper Quaternary sediments of the eastern equatorial Pacific. *Marine Geology*, *120*(3), 327–333. https://doi.org/10.1016/0025-3227(94)90065-5

Sweetman, A. K., Smith, A. J., de Jonge, D. S. W., Hahn, T., Schroedl, P., Silverstein, M., Andrade, C., Edwards, R. L., Lough, A. J. M., Woulds, C., Homoky, W. B., Koschinsky, A., Fuchs, S., Kuhn, T., Geiger, F., & Marlow, J. J. (2024). Evidence of dark oxygen production at the abyssal seafloor. *Nature Geoscience*, *17*(8), 737–739. https://doi.org/10.1038/s41561-024-01480-8

Turner, P. J. (2019). Deep-Sea Mining and Environmental Management. In J. K. Cochran, H. J. Bokuniewicz, & P. L. Yager (Eds.), *Encyclopedia of Ocean Sciences (Third Edition)* (pp. 507–515). Academic Press. https://doi.org/10.1016/B978-0-12-409548-9.11106-6

Usui, A., Nishimura, A., & Mita, N. (1993). Composition and growth history of surficial and buried manganese nodules in the Penrhyn Basin, Southwestern Pacific. *Marine Geology*, *114*(1), 133–153. https://doi.org/10.1016/0025-3227(93)90044-V

Valsangkar, A. B., & Rebello, J. M. S. (2016). Regional Variability in Occurrence and Distribution of Polymetallic Nodules in the Central Indian Basin. *Marine Georesources & Geotechnology*, *34*(6), 542–549. https://doi.org/10.1080/1064119X.2015.1033503

Wakefield, J. R., & Myers, K. (2018). Social cost benefit analysis for deep sea minerals mining. *Marine Policy*, *95*, 346–355. https://doi.org/10.1016/j.marpol.2016.06.018

Wegorzewski, A. V., Grangeon, S., Webb, S. M., Heller, C., & Kuhn, T. (2020). Mineralogical transformations in polymetallic nodules and the change of Ni, Cu and Co crystal-chemistry upon burial in sediments. *Geochimica et Cosmochimica Acta*, *282*, 19–37. https://doi.org/10.1016/j.gca.2020.04.012